J Therm Anal Calorim (2010) 102:1079–1086
DOI 10.1007/s10973-010-0899-1

Structural characterization, thermal investigation, and liquid crystalline behavior of 4-[(4-chlorobenzyl)oxy]-3,4′-dichloroazobenzene

Anca Moanţă · Cătălina Ionescu · P. Rotaru · Margareta Socaciu · Ana Hărăbor

Received: 7 March 2010 / Accepted: 17 May 2010 / Published online: 4 June 2010
© Akadémiai Kiadó, Budapest, Hungary 2010

Abstract Using the Williamson method, a new dye 4-[(4-chlorobenzyl)oxy]-3,4′-dichloroazobenzene (CODA) with liquid crystalline properties was synthesized. The structure and the thermal behavior of CODA were investigated by means of nuclear magnetic resonance, X-ray diffraction, differential scanning calorimetry, and light polarized optical microscopy techniques. The thermophysical processes were monitored by heating–cooling cycles, but the formation of liquid crystal phases were exhibited only for small values of the cooling rates. For the first heating–cooling cycle, the melting and the solidification processes, thus the characteristic temperatures, are shifted to higher values when compared to the following cycles.

Keywords Azomonoethers · DSC · NMR · LPOM · Liquid crystals · Phase transitions · Thermal analyses

Introduction

Thermal analyses of new compounds used as precursors for nanostructured materials synthesis or designed for temperature controlled applications like dyes exhibiting liquid crystalline nature [1–8] are a real need and an advantageous pointer before trying to functionalize them [9–14]. From the point of view of possible applications (e.g., liquid crystals for non-linear optics applications or for dye lasers) [15–17], azomonoethers are a large interest class of dyes.

We have reported the synthesis, spectral characterization [18–20], and thermal stability [21–29] of some synthetic azoic dyes, which have a 4-[(4-chlorobenzyl)oxy]azobenzene derived structure. These compounds were synthesized using the Williamson etherification method [18, 19], by condensation of 4-chloromethyl chlorobenzene with sodium salts of 4-(phenylazo)phenols. One of the compounds we have synthesized is 4-[(4-chlorobenzyl)oxy]-3,4′-dichloroazobenzene (CODA). In this article, the thermal behavior and the structure of CODA are reported, using differential scanning calorimetry (DSC), nuclear magnetic resonance (NMR), X-ray diffraction (XRD), and light polarized optical microscopy (LPOM) techniques. For the CODA compound the liquid crystalline properties were exhibited in the characteristic the temperature ranges and the thermophysical parameters were determined.

Experimental

Synthesis of 4-[(4-chlorobenzyl)oxy]-3,4′-dichloroazobenzene

To a one-necked round-bottomed flask equipped with a mechanical stirrer, thermometer, and condenser, 2-chloro-4-(4-chloro-phenylazo)-phenol, NaOH (Fluka pellets 100%) and C_2H_5OH (Fluka absolute)–C_6H_6 (Fluka 99%) mixture (3:1, in volumes) were added. 2-chloro-4-(4-chloro-phenylazo)-phenol was synthesized by coupling the diazonium salt of 4-chloro-aniline (Fluka 97%) with 2-chloro-phenol (Fluka 98%). The reaction mixture was

A. Moanţă · C. Ionescu
Faculty of Chemistry, University of Craiova, Calea Bucuresti Str., Nr. 107 I, Craiova, Romania

P. Rotaru (✉) · M. Socaciu · A. Hărăbor
Faculty of Physics, University of Craiova, A.I. Cuza Str., Nr. 13, Craiova, Romania
e-mail: protaru@central.ucv.ro; petrerotaru@yahoo.com

stirred 2 h at 343 K, until the 2-chloro-4-(4-chloro-phenylazo)-phenol has reacted with sodium hydroxide. By the distillation of azeotropic mixture ethanol–benzene–water, the reaction water was removed. 4-chloromethyl chlorobenzene (Fluka 98%) was added to anhydrous azophenoxide (Fluka 99%) and the reaction mixture was stirred 4 h at 323–328 K. After cooling at room temperature, the solid product was filtered, washed with water in order to remove the sodium chloride and dried further in a heating chamber at 378 K. The reaction product was recrystallized from C_2H_5OH (Fluka absolute) to $C_6H_5CH_3$ (Fluka 99%) (2:1, in volumes), providing 77.5% yield of CODA.

Characterization methods and techniques

All NMR spectra were recorded at 293 K on a Bruker DRX-400 spectrometer working at 400.13 MHz for ^{1}H and 100.62 MHz for ^{13}C. The chemical shifts (δ) of ^{1}H and ^{13}C spectra are reported in ppm/TMS, with the ^{1}H and ^{13}C chloroform signals at 7.26 and 77.00 ppm, respectively. The coupling constants (J) are reported in Hz. 1D spectra (^{1}H-and ^{13}C-APT) and 2D spectra of homonuclear (COSYGP) and inverse heteronuclear (HMQCGP) correlations were recorded with the standard BRUKER sequences.

XRD measurements were performed on powder samples, with a Shimadzu XRD-6000 X-ray diffractometer, equipped with a vertical goniometer and a scintillation detector. The functioning parameters of the X-ray tube (A40-Cu type) were set to 40 kV and an electric current intensity of 30 mA. A continuous scan measurement has been chosen as operating mode in a geometry ($\theta/2\theta$) setting a scan rate of 1° 2θ min^{-1} and a scan range from 2 to 37.5° 2θ. Divergence slit was of 1.0000°, scattering slit was of 1.0000°, and receiving slit of 0.1500 mm.

DSC studies of CODA compound were carried out in dynamic air atmosphere (150 cm^3 min^{-1}), under combined non-isothermal linear and isothermal regimes. A horizontal "Diamond" Differential/Thermo gravimetric Analyzer from PerkinElmer Instruments was used during the measurements. The enthalpic calculations were performed with the specialized software "Pyris."

Optical microstructural observations were made with a polarizing microscope LEICA DM 2500 P, equipped with a video-recorder camera and a hot thermostated stage TMS 94 (Linkam Scientific Instruments Ltd.) connected to the temperature programmer. The new synthesized compound was introduced between two parallel glass plates (a slide and a coverslip) without any particular care and was examined between crossed polarisers under a polarizing microscope [29]. The heating and cooling cycles were performed with the rates of 2 K min^{-1} each.

Results and discussion

Structural characterization by NMR and XRD techniques

The unconventional numbering system (Fig. 1) of CODA was chosen for an easier understanding of the signals in the NMR spectra.

The proton spectrum of this molecule contains one singlet, one AMX system, and two AA′BB′ systems due, respectively, to the methylene group, the ring A, and the two *para*-disubstituted benzene rings B and C (Fig. 2).

The two doublets at 8.02 ($J = 2.4$ Hz) and 7.06 ppm ($J = 8.8$ Hz) belong obviously to H_2 and H_5, respectively. The COSY spectrum (Fig. 3) shows that the third signal of the AMX system is at 7.83, mixed with the AA′ part of the AA′BB′ system with the largest $\Delta\nu_{AB}$.

The moiety at 7.83 ppm of this AA′BB′ system belongs to H_a and $H_{a'}$ which are *ortho* to the azo group, known to be a more *ortho* deshielding group than chlorine [30]. The other half of this system being at 7.47 ppm, it is almost an AA′XX′ system at 400 MHz.

On the contrary, ring C is substituted with two groups of similar substituent effects [30] and the $\Delta\nu_{AB}$ of the AA′BB′ system is small, even at 400 MHz. Thus, the system was simulated with gNMR [31] to obtain the correct chemical shifts shown in Table 1. It may be noticed that the high-frequency moiety of the AA′BB′ system is slightly

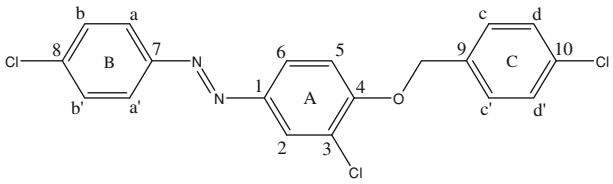

Fig. 1 Structure of CODA and employed numbering system

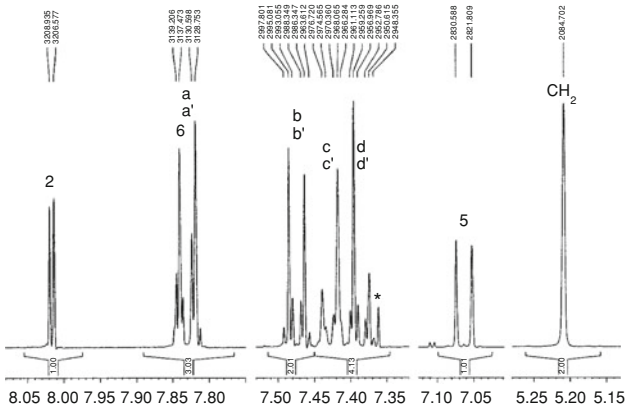

Fig. 2 ^{1}H-NMR spectrum of 4-[(4-chlorobenzyl)oxy]-3,4′-dichloroazobenzene in $CDCl_3$

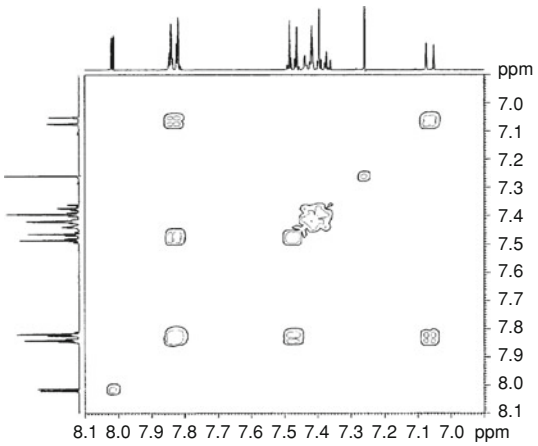

Fig. 3 COSY (^{1}H–^{1}H) spectrum of CODA (aromatic region only)

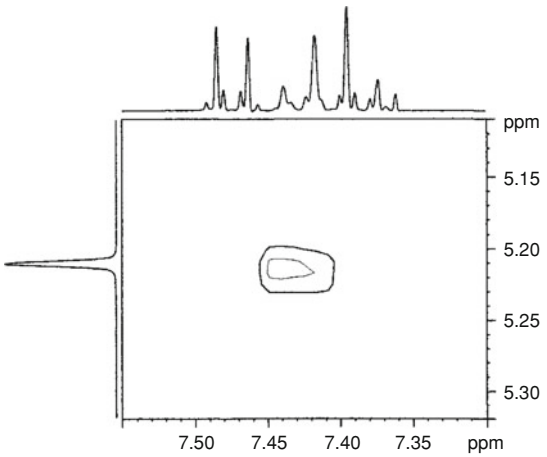

Fig. 4 COSY spectrum of CODA. Expansion of the cross-peak between the AA′BB′ system of ring C and the CH_2 group

Table 1 ^{1}H- and ^{13}C-NMR parameters of CODA

^{1}H		^{13}C	
–	–	C_1	146.76[a]
H_2	8.017	C_2	123.24
–	–	C_3	124.20[a]
–	–	C_4	156.12[a]
H_5	7.063	C_5	113.08
H_6	7.832	C_6	124.90
–	–	C_7	150.69[a]
–	--	C_8	136.77[b]
–	–	C_9	134.31[b]
–	–	C_{10}	134.02[b]
H_a and $H_{a'}$	7.830	C_a and $C_{a'}$	123.99
H_b and $H_{b'}$	7.474	C_b and $C_{b'}$	129.31
H_c and $H_{c'}$	7.427	C_c and $C_{c'}$	128.39
H_d and $H_{d'}$	7.388	C_d and $C_{d'}$	128.87
CH_2	5.210	CH_2	70.14

[a] These assignments were realized on the basis of calculations using additive substituent effects [38]

[b] These assignments may be interchanged

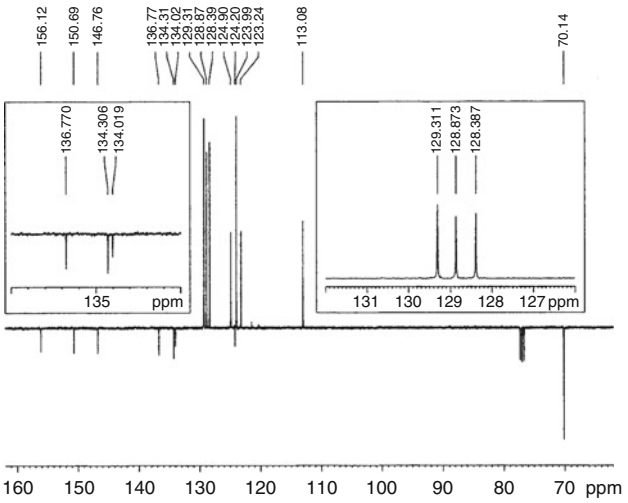

Fig. 5 ^{13}C-APT spectrum of CODA in $CDCl_3$

broadened by a long range coupling constant with the *ortho* CH_2 group, allowing its assignment to the pair $H_c-H_{c'}$. This scalar interaction is confirmed by the COSY spectrum (Fig. 4).

For ^{13}C analysis, a ^{13}C-APT experiment was recorded, based on the JMOD pulse sequence which separates the signals of primary and tertiary atoms from the signals of secondary and quaternary atoms by giving them different phases (Fig. 5).

The CH carbon signals were assigned using the inverse 2D heteronuclear correlation spectrum HMQC (Fig. 6) and the results are shown in Table 1.

The XRD analysis is a good method to evaluate the long range structural ordering or periodicity of the material [32].

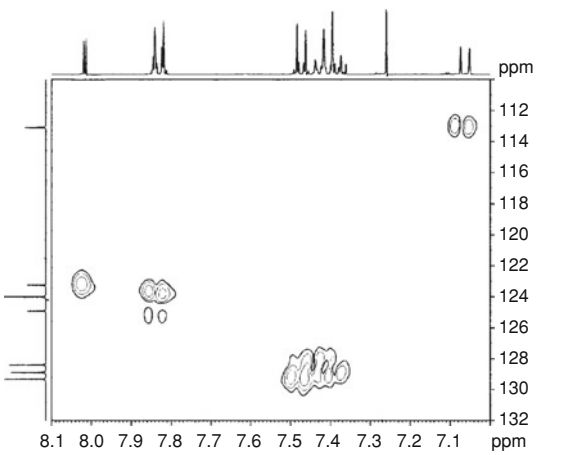

Fig. 6 Heterocorrelation (^{1}H–^{13}C) spectrum of CODA (tertiary atoms region only)

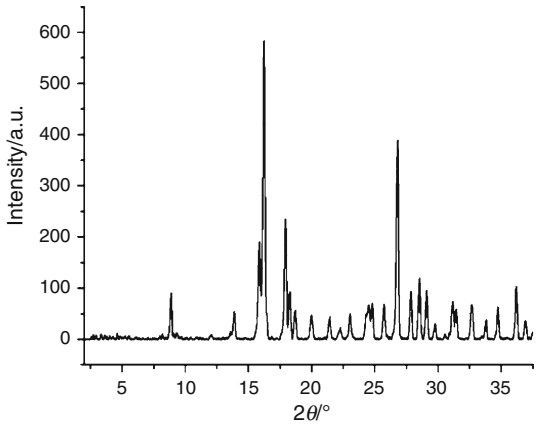

Fig. 7 XRD patterns of CODA in 7–37.5° (2θ) range

Table 2 Main XRD peaks of CODA

Relative intensity/a.u.	d/Å	2θ/°	*hkl*
100	5.46009	16.222	200
67	3.35018	26.854	301
40	4.97040	17.815	020
33	5.58152	15.865	111
20	3.094639	28.800	031
18	2.47705	36.260	023
16	3.19223	27.945	212
16	2.97739	30.015	131
15	9.95619	8.875	010

In the case of CODA, the Bragg diffraction patterns obtained for $\lambda = 1.54059$ Å Cu $K\alpha_1$ X-ray radiation, indicate a good crystallinity (Fig. 7).

Our results have been compared with those in the JCPDS database at the International Centre for Diffraction Data. For indexing the diffraction patterns of this new material, we were guided by a orthorhombic similar structure which may be found in the cards 20-1271 [33] and 47-2210 [34].

Table 2 shows for the main XRD peaks of CODA: the relative intensity, the interplanar distance (d), the diffraction angles (2θ), and the Miller indexes (*hkl*) of the diffraction planes.

The unit cell of CODA material was indexed as orthorhombic structure and the calculated experimental lattice parameters were: $a = 10.920$ Å, $b = 9.956$ Å, and $c = 8.567$ Å; this proves a long range structural organization degree.

Concerning the average crystallite sizes when using the Scherrer formula [32, 35], there are some approximation methods to define the peak width (B), resulting different values for the K constant in the Scherrer formula. When assuming ellipsoidal particles, it was found [35] that the much empirical approach of Jones will provide the best means for making allowance for the dimensions of the samples. In this last case, by using the integral widths B_I when $K_I = 1.333$, we have obtained for the particles dimensions of CODA the mean value of about 1.21 nm.

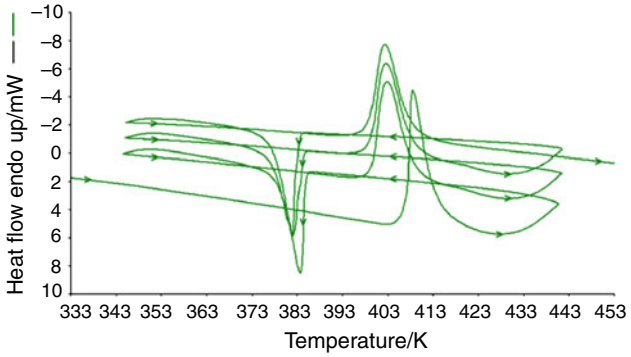

Fig. 8 DSC heating–cooling cycles of CODA for 10 K min^{-1}

Thermal study of CODA by differential scanning calorimetry

In order to determine the thermal stability domain and to identify the phase transitions of the investigated compound, heating–cooling cycles were imposed by alternating non-isothermal linear temperature programs of ±10 K min^{-1} with 10 min isothermal regimes at the starting (343 K) and ending (443 K) temperatures. Beginning with the forth cycle, only the melting has been realized, the temperature increasing with 10 K min^{-1} until 600 °C. The compound is stable until 200 °C; afterward, it decomposes entirely in two steps up to 580 °C.

The DSC curve of the heating–cooling cycles for 10 K min^{-1} is shown in Fig. 8.

For the part of the experiment which corresponds to the heating, an endothermic effect representing the melting of the compound is observed, while for the cooling one, the exothermic peaks are characteristic to its solidification. In the first cycle the compound is stabilized, the transformation peaks being different from the other cycles (for the melting and for the solidification as well). The thermophysical parameters of the melting and solidification of CODA, obtained by means of the DSC heating–cooling cycles (at 10 K min^{-1}) are shown in Table 3.

The melting temperature in the first cycle is with 6 K greater than for the following cycles, while the solidification temperature in the first cycle is with about 1.5 K greater than in the other cycles. The displacement of the melting process to higher temperatures in the first heating cycle can be explained by the supplementary strength that the crystalline structure introduces. The enthalpy variations of the melting (endothermic) and solidification (exothermic) processes are not much different from one cycle to the

Table 3 Thermophysical parameters of CODA for the DSC heating–cooling cycles at 10 K min^{-1}

Cycle	Process	Temperature range/K	ΔH/kJ kg^{-1}	T_{max}/K	Process	Temperature range/K	ΔH/kJ kg^{-1}	T_{max}/K
First	Melting	403.2–425.7	97.96	408.6	Solidification	386.0–3374.0	−80.42	383.6
Second	Melting	396.3–428.0	102.73	402.8	Solidification	384.2–372.7	−80.19	382.1
Third	Melting	394.7–427.7	103.43	402.6	Solidification	384.5–372.4	−80.33	382.0
Fourth	Melting	393.1–417.5	100.71	402.3	–	–	–	–

other. Only for the first cycle, the melting peak is sharper and the thermal effect is smaller, being enhanced by the actual higher temperatures. After stabilization, the compound properties repeat rigorously in the other cycles.

Since the temperature variation rates of 10 K min^{-1} are too large, the characteristic liquid crystalline mesophases do not appear. The additional phase transitions can be observed only for smaller variation rates of the temperature, when thermophysical processes would separate. Therefore, the cooling processes should be further investigated, these transformations happening in quite narrower temperature ranges.

The second experiment used a temperature program of two complete heating–cooling cycles (rates of 2 K min^{-1}) in the temperature range of 323–433 K, intercalated by 10 min maintaining the temperature to the initial (323 K) and final (433 K) values. Further with the third cycle, after melting the investigated compound, the temperature continued to increase by 2 K min^{-1} up to 873 K.

The DSC curve (heat flow curve) and the imposed temperature variation of the sample in time are shown in Fig. 9.

At lower values of temperature variation rates (for example, as here for 2 K min^{-1}), the liquid crystal properties of CODA can exhibited by the DSC measurements. In the first cycle, at heating, the melting is produced and the isotropic liquid phase is obtained. For the first cycle as well, but at cooling (Fig. 10), the liquid crystal phase is generated at 383.0 K in the isotropic liquid and from 382.0 K, the transition to the solid crystalline phase is produced.

At cooling in the second cycle (Fig. 11), the thermal behavior of CODA is different from the one in the first cycle, because the solidification process is displaced with temperature. In Fig. 11, the thermal effect of the liquid crystal formation is apparently bigger than the thermal effect of the solidification. This statement is not true, since from 384.1 to 381.3 K, the solidification takes place simultaneously with the liquid crystal phase transformation (with maxima at 383.9 and 381.9 K). Between 381.3 and 378.0 K, the (re)crystallization of CODA follows.

This kind of behavior is expected, since for the first heating–cooling cycle, the powder used was the one obtained straight from the organic synthesis, which has a rather different microstructure (than the solid after the first

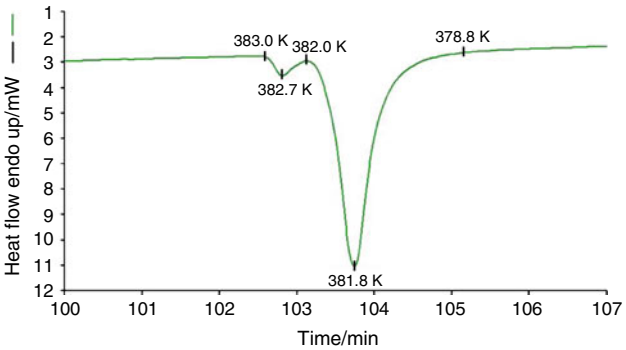

Fig. 10 DSC cooling curve of CODA for the first cycle at 2 K min^{-1}

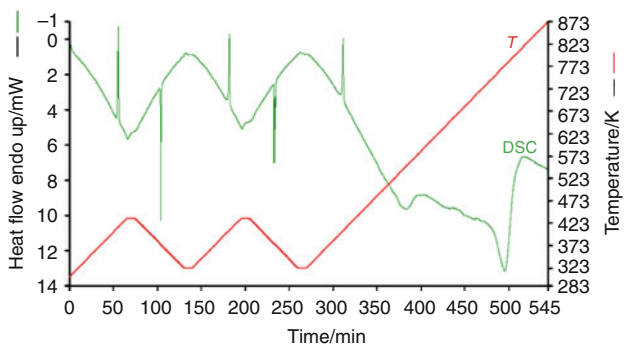

Fig. 9 Heat flow and temperature of the sample versus time ($\beta = \pm 2$ K min^{-1})

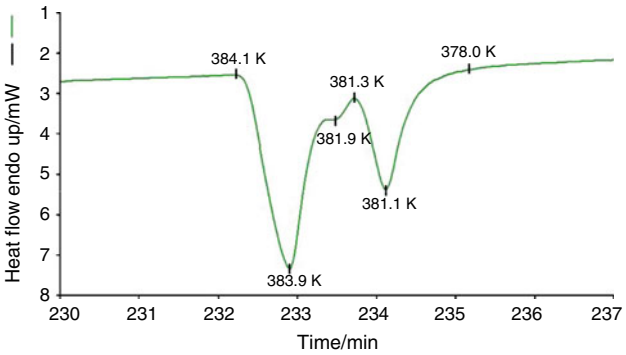

Fig. 11 DSC cooling curve of CODA for the second cycle at 2 K min^{-1}

Table 4 Thermophysical parameters of CODA at 2 K min^{-1}

Cycle	Process	Temperature range/K	ΔH/kJ kg^{-1}	T_{max}/K	Process	Temperature range/K	$\sum\Delta H$/kJ kg^{-1}	T_{max}/K
First	Melting	404.5–412.6	92.03	407.8	Phase transition	383.0–382.0	−79.72	382.7
					Solidification + crystallization	382.0–378.0		381.8
Second	Melting	397.6–405.8	87.56	401.5	Phase transition + solidification	384.1–381.3	−80.77	383.9
					Crystallization	381.3–378.0		381.1
Third	Melting	396.5–405.3	83.99	401.3	–	–	–	–

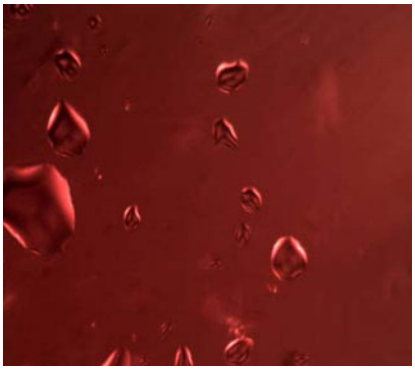

Fig. 12 Small droplets in the homeotropic isotrope liquid matrix (cooling, 383.1 K)

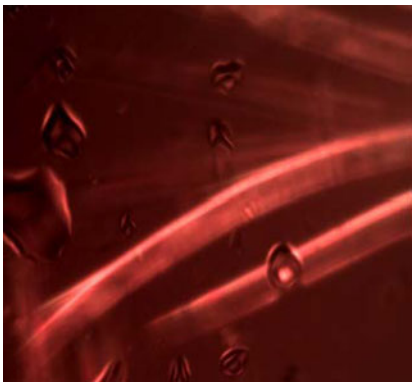

Fig. 14 Batonnets shape, as simple cylinders with only one straight disclination line (cooling, 382.0 K)

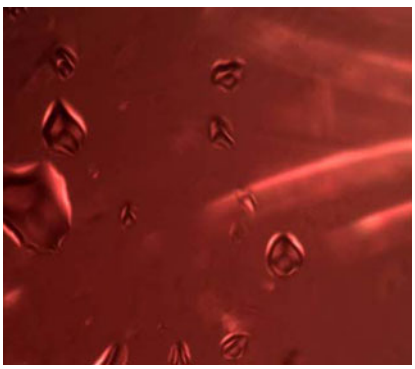

Fig. 13 Growth of the batonnets' texture together with the droplets texture (cooling, 382.7 K)

Fig. 15 Coalescence and shape reorganization of the batonettes (cooling, 380.0 K)

recrystallization in the DSC) and has retained small amounts of solvent.

The thermophysical parameters obtained by means of the DSC analysis in the heating–cooling cycles at 2 K min^{-1} are shown in Table 4. As in the first experiment at higher temperature variation rate, the melting point is about 6–6.5 K displaced to higher temperature values.

For the cooling part of the second experiment, the solidification can occur together with the crystallization—first cycle, or together with the liquid phase transition—second cycle (Table 4), but the total enthalpy variation is constant for each cycle ($\Sigma\Delta H \approx 80$ kJ kg^{-1}); the same thermophysical processes are therefore suggested to occurred, with only the solidification one shifting to higher or lower temperatures.

These processes can be also observed using an optical microscope with polarized light, confirming the results obtained by the two DSC experiments. At cooling in first cycle, from the isotropic melt a few droplets (spherulitic domains) appear near the clearing point, as in Fig. 12. Furthermore, the formation of batonnets follows (Fig. 13).

For most droplets the spherical symmetry is reduced to revolution symmetry by a focal domain attached at the center [36]. In its initials state, the batonnets may be simple

Fig. 16 Reticular or fan shaped texture of the batonnets (cooling, 376.8 K)

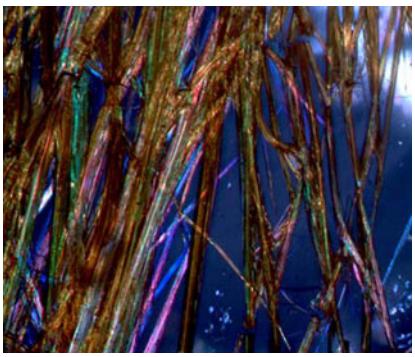

Fig. 17 The batonnets (cooling, 378.0 K)

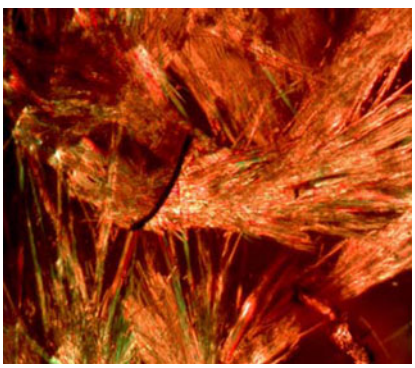

Fig. 18 Solid paramorphe texture, with small homeotropic domains of isotropic phase, before clearing point (heating, 398.6 K)

cylinder with only one straight disclination line, as in Fig. 14. During its growth, two or more batonnets meet and they may coalesce, sometimes textures of exotic shape resulting [37] as in Fig. 15. During further growth, the batonnets often coalesce and may reorganize its shape until a final fan shaped or reticular texture like in Fig. 16 is established.

In Fig. 17, it is shown that the image of CODA crystals at cooling in the second cycle, with batonnets which coalesce in exotic texture.

The crystals in Fig. 17 appearing at cooling, should finally look like the solid paramorphe texture with the small homeotropic domains of isotropic phase (Fig. 18), image which was obtained at heating in the second cycle, just before the clearing point.

Conclusions

A new azomonoetheric dye CODA with liquid crystalline properties has been synthesized. Detailed ^{1}H- and ^{13}C-NMR study (400 MHz) of CODA compound using mono and bidimensional NMR spectra was reported. The results are in agreement with the considered molecular structure. By XDR analysis, the main diffraction maxima of the CODA compound have been identified since it has exhibited a good crystallinity and the size of crystallite was established. CODA compound has been indexed as crystallizing in orthorhombic symmetry. The thermophysical processes were monitored by heating–cooling cycles, but the formation of liquid crystal phases were observed only for small values of the cooling rates, when they would separate. When realizing heating–cooling cycles with the temperature variation rate of 10 K min^{-1}, mesomorphic transitions do not appear in the isotropic liquid phase and all processes are gathered under the same DSC peak. For the first heating–cooling cycle, the melting and the solidification processes are shifted to higher values when compared to the following cycles. The crystalline structure influences this first cycle, the melting temperature being with 6 K greater than for the following cycles, while the solidification temperature in the first cycle is with approximately 1.5 K greater than in the other cycles. For the 2 K min^{-1} experiment, in the cooling part, the liquid crystalline phase transition was identified. In this part of the experiment, solidification of CODA can occur together with the crystallization—first cycle, or together with the liquid phase transition—second cycle. This temperature displacement of the solidification is highlighted by the total enthalpy variation which preserves its value for each cycle ($\Sigma\Delta H \approx 80$ kJ kg^{-1}) and by optical microscopy images collected at precise temperatures during cooling.

Acknowledgements The authors are grateful to Andrei Rotaru (INFLPR Bucharest/University of St Andrews), Prof. Alain Fruchier (Ecole Nationale Supérieure de Chimie, Montpellier), and Diego Carnevale and Karen Johnston (University of St Andrews) for their useful discussions and the help they provided in writing this article.

References

1. Tian ZR, Voigt JA, Liu J, McKenzie B, McDermott MJ, Rodriguez MA, Konishi H, Xu H. Complex and oriented ZnO nanostructures. Nat Mater. 2003;2(12):821–6.
2. Gerstel P, Hoffmann RC, Lipowsky P, Jeurgens LPH, Bill J, Aldinger F. Mineralization from aqueous solutions of zinc salts directed by amino acids and peptides. Chem Mater. 2005;18(1):179–86.
3. Bauermann LP, Bill J, Aldinger F. Bio-friendly synthesis of ZnO nanoparticles in aqueous solution at near-neutral pH and low temperature. J Phys Chem B. 2006;110(11):5182–5.
4. Kropidłowska A, Rotaru A, Strankowski M, Becker B, Segal E. Thermal stability and non-isothermal decomposition kinetics of a heteroleptic cadmium(II) complex, potential precursor for semiconducting CdS layers. J Therm Anal Calorim. 2008;91(3):903–9.
5. Gűr M, Kocaokutgen H, Taş M. Synthesis, spectral, and thermal characterisations of some azo-ester derivatives containing a 4-acryloyloxy group. Dye Pigment. 2007;72(1):101–8.
6. Badea M, Emandi A, Marinescu D, Cristurean E, Olar R, Brăileanu A, Budrugeac P, Segal E. Thermal stability of some azo-derivatives and their complexes—1-(2-benzothiazolyl)-3-methyl-4-azo-pyrazil-5-one derivatives and their Cu(II) complexes. J Therm Anal Calorim. 2003;72(2):525–31.
7. Dincalp H, Toker F, Durucasu J, Avcibasi N, Icli S. New thiophene-based azo ligands containing azo methine group in the main chain for the determination of copper (II) ions. Dye Pigment. 2007;75(1):11–24.
8. Chen Z, Wu Y, Gu D, Gan F. Nickel(II) and copper(II) complexes containing 2-(2-(5-substituted isoxazol-3-yl)hydrazono)-5, 5-dimethylcyclohexane-1, 3-dione ligands: synthesis, spectral and thermal characterizations. Dye Pigment. 2008;76(3):624–31.
9. Lin CC, Li YY. Synthesis of ZnO nanowires by thermal decomposition of zinc acetate dihydrate. Mater Chem Phys. 2009;113(1):334–7.
10. Rotaru A, Mietlarek-Kropidłowska A, Constantinescu C, Scărişoreanu N, Dumitru M, Strankowski M, Rotaru P, Ion V, Vasiliu C, Becker B, Dinescu M. CdS thin films obtained by thermal treatment of cadmium (II) complex precursor deposited by matrix assisted pulsed laser evaporation technique. Appl Surf Sci. 2009;255(15):6786–9.
11. Rotaru A, Constantinescu C, Mândruleanu A, Rotaru P, Moldovan A, Győryová K, Dinescu M, Balek V. Matrix assisted pulsed laser evaporation of zinc benzoate for ZnO thin films and non-isothermal decomposition kinetics. Thermochim Acta. 2010;498(1–2):81–91.
12. Rotaru A, Constantinescu C, Rotaru P, Moanţă A, Dumitru M, Dinescu M, Segal E. Thermal analysis and thin films deposition by matrix assisted pulsed laser evaporation of a 4CN type azomonoether. J Therm Anal Calorim. 2008;92(1):279–84.
13. Barbera J, Giorgini L, Paris F, Salatelli E, Tejedor RM, Angiolini L. Supramolecular chirality and reversible chiroptical switching in new chiral liquid-crystal azopolymers. Chem Eur J. 2008;14(35):11209–21.
14. Benmouna R, Benyoucef B. Thermophysical and thermomechanical properties of Norland optical adhesives and liquid crystal composites. J Appl Polym Sci. 2008;108(6):4072–9.
15. Chao TY, Chang HL, Su WC, Wu JY, Jeng RJ. Nonlinear optical polyimide/montmorillonite nanocomposites consisting of azobenzene dyes. Dye Pigment. 2008;77(3):515–24.
16. Lu M, Cunningham BT, Park SJ, Eden JG. Vertically emitting, dye-doped polymer laser in the green (lambda similar to 536 nm) with a second order distributed feedback grating fabricated by replica molding. Opt Commun. 2008;281(11):3159–62.
17. Oliveira-Campos AMF, Oliveira MJ, Rodrigues LM, Silva MM, Smith MJ. Thermal analysis of a polymorphic azo dye derived from 2-amino-5-nitrothiazole. Thermochim Acta. 2007;453(1):52–6.
18. Radu S, Şarpe-Tudoran C, Jianu A, Rău G. Aromatic azomonoethers as new organic materials for nonlinear optics. Rev Roum Chim. 1998;43:735–9.
19. Radu S, Moanţă A, Rău G. 4-[(4-chlorobenzyl)oxy]-azobenzenes. Rev Chim (Bucureşti). 2001;52(11):619–22.
20. Moanţă A, Radu S, Rău G. Studiul proprietăţilor spectrale şi determinarea activităţii biologice pentru o serie de 4-[(4-clorobenzil)oxi]-azobenzeni. Rev Chim (Bucureşti). 2007;58(2):229–31.
21. Rotaru A, Moanţă A, Sălăgeanu I, Budrugeac P, Segal E. Thermal decomposition kinetics of some aromatic azomonoethers. Part I. Decomposition of 4-[(4-chlorobenzyl)oxy]-4′-nitro-azobenzene. J Therm Anal Calorim. 2007;87(2):395–400.
22. Rotaru A, Kropidłowska A, Moanţă A, Rotaru P, Segal E. Thermal decomposition kinetics of some aromatic azomonoethers. Part II. Non-isothermal study of three liquid crystals in dynamic air atmosphere. J Therm Anal Calorim. 2008;92(1):233–8.
23. Rotaru A, Moanţă A, Rotaru P, Segal E. Thermal decomposition kinetics of some aromatic azomonoethers. Part III. Non-isothermal study of 4-[(4-chlorobenzyl)oxy]-4′-chloro-azobenzene in dynamic air atmosphere. J Therm Anal Calorim. 2009;95(1):161–6.
24. Rotaru A, Moanţă A, Popa G, Rotaru P, Segal E. Thermal decomposition kinetics of some aromatic azomonoethers. Part IV. Non-isothermal kinetics of 2-allyl-4-((4-(4-methylbenzyloxy) phenyl)diazenyl) phenol in dynamic air atmosphere. J Therm Anal Calorim. 2009;97(2):485–91.
25. Rotaru A, Jurca B, Moanţă A, Sălăgeanu I, Segal E. Kinetic study of thermal decomposition of some aromatic ortho-chlorinated azomonoethers. 1. Decomposition of 4[(2-chlorobenzyl)oxi]-4′-trifluoromethyl-azobenzene. Rev Roum Chim. 2006;51(5):373–8.
26. Rotaru A, Kropidłowska A, Rotaru P. On the inappropriate fit of diffusion functions at thermal decomposition of some azomonoethers in liquid state. Phys AUC. 2007;17(2):115–8.
27. Rotaru A, Brătulescu G, Rotaru P. Thermal analysis of azoic dyes; Part I. Non-isothermal decomposition kinetics of [4-(4-chlorobenzyloxy)-3-methylphenyl](p-tolyl)diazene in dynamic air atmosphere. Thermochim Acta. 2009;489:63–9.
28. Rotaru A, Goşa M, Segal E. Isoconversional linear integral kinetics of the non-isothermal evaporation of 4-[(4-chlorobenzyl)oxy]-4′-trifluoromethyl-azobenzene. Stud Univ Babeş-Bolyai Chem. 2009;3:185–92.
29. Demus D, Richter L. Textures of liquid crystals. 2nd ed. Leipzig: Verlag Chemie; 1978.
30. Pretsch E, Bühlmann P, Affolter C. Structure determination of organic compounds: tables of spectral data. Berlin: Springer; 2000.
31. Budzelaar PHM. gNMR 5.0. Oxford: IvorySoft; 2006.
32. Cavalcante LS, Marques VS, Sczancoski JC, Escote MT, Joya MR, Varela JA, Santos MRMC, Pizani PS, Longo E. Synthesis, structural refinement and optical behavior of $CaTiO_3$ powders: a comparative study of processing in different furnaces. Chem Eng J. 2008;143:299–307.
33. Bressot C. Ammonium thotium oxalate hydrate. Bull Soc Chim Fr. 1966;70:2094–7.
34. Warhadpande S, Gupta M. Poly(acetanilide)perchlorate. Indian J Chem. 1992;31:43–9.
35. Patterson AI. The Scherrer formula for X-Ray particle size determination. Phys Rev. 1939;56:978–82.
36. Gray GW, Goodby JWG. Smectic liquid crystals. Textures and structures. Philadelphia: Leonard Hill; 1984.
37. Bouligand Y. Defect and textures. In: Demus D, Goodby JWG, Gray GW, Spiess HW, Vill V, editors. Handbook of liquid crystals, vol. I. New York: Wiley-VCH; 1998. p. 406–54.
38. Ewing DF. 13C substituent effects in monosubstituted benzenes. Org Magn Reson. 1979;12:499–524.